Low-Complexity Neural Networks for Denoising Imperfect CSI in Physical Layer Security

Idowu Ajayi, Yahia Medjahdi, Lina Mroueh, Olumide Okubadejo, Fatima Zohra Kaddour

Low-Complexity Neural Networks for Denoising Imperfect CSI in Physical Layer Security

Idowu Ajayi*, Yahia Medjahdi¶, Lina Mroueh*, Olumide Okubadejo‡ and Fatima Kaddour†

*Institut Supérieur d'Électronique de Paris (ISEP), Paris, France
¶IMT Nord Europe, Institut Mines-Télécom, Univ. Lille, Centre for Digital Systems, F-59000 Lille, France
‡ École Supérieure d'Ingénieurs en Électrotechnique et Électronique (ESIEE), Paris, France
†Agence Nationale des Fréquences (ANFR), Maisons-Alfort, France
Corresponding author: Idowu Ajayi (idowu.ajayi@isep.fr)

***Abstract*—Channel adaptation physical layer security (PLS) schemes are degraded when the channel state information (CSI) is imperfect. Imperfect CSI is due to factors such as noisy feedback, outdated CSI, etc. In this paper, we propose a low-complexity noisy CSI denoising scheme based on the autoencoder architecture of deep neural networks referred to as DenoiseSecNet. To further reduce complexity, we then propose a hybrid version (HybDenoiseSecNet) that combines a legacy denoising scheme and a shallow neural network to achieve a similar performance as DenoiseSecNet. Simulation results, in terms of bit error rate (BER), secrecy capacity, and normalized mean squared error (NMSE), show the performance improvement of our proposed scheme compared to conventional denoising schemes. Finally, we study the significant reduction in computational complexity of the proposed scheme compared to another neural network scheme.**

***Index Terms*—Autoencoder, deep learning, matched filter (MF) precoding, neural networks, orthogonal frequency division multiplexing (OFDM), and physical layer security (PLS).**

I. Introduction and Motivations

Physical layer security (PLS) is a concept that has gained a lot of attention in recent times. It uses wireless channel characteristics such as noise, fading, diversity, etc. as a source of security. Channel adaptation is a category of PLS techniques in which the transmitter (Alice) tunes the transmission parameters to favor the legitimate receiver (Bob) while remaining random to or degrading the eavesdropper (Eve) [1]. Channel adaptation techniques require knowledge of instantaneous channel state information (CSI). However, the instantaneous CSI is not usually perfect due to factors such as noisy feedback, outdated CSI, etc. This means that under imperfect CSI conditions, the performance of the PLS scheme deteriorates.

Several denoising strategies have been considered in the literature. Denoising is the process of removing noise from a noisy signal. In [2], the use of the truncation technique to denoise the noisy CSI was presented. In this method, the authors assumed that the channel length is known and only the channel impulse response (CIR) taps below the channel length are considered significant. The CIR is truncated at this point and all other taps beyond this are discarded. It was shown to give a better mean squared error (MSE) compared to the no truncation case. More popular is the noisy CSI denoising using the threshold approach. Several works have been done in this area as seen in [3], [4]. An iterative threshold method using convolutional code for channel estimation in an orthogonal frequency division multiplexing (OFDM) transmission was proposed in [3]. The results showed that higher transmit diversity gains and better bit error rate (BER) performances were achieved compared to legacy estimation schemes that are more susceptible to noise. In [4], an efficient time-domain threshold-based channel estimation technique was proposed in OFDM systems. The threshold, referred to as the universal threshold, can be applied without prior knowledge of the channel statistics and the standard deviation of the noise.

Recently, deep learning has been adopted in many fields such as natural language processing [5], computer vision [6], etc. Similarly, researchers have started working on the use of deep learning for CSI prediction (in the case of outdated CSI [7]) or CSI denoising (in the case of noisy CSI [8], [9]). The authors in [8] proposed an autoencoder to reduce CSI feedback in a massive MIMO system operating in frequency division duplex (FDD) mode. The CSI is encoded after CSI estimation and then transmitted as a low-dimensional codeword. At the receiver, the received codeword is decoded to recover the original CSI. A noise extraction unit (NEU) was then used to extract the noise in the codeword. The model predicts the noise and then subtracts the predicted noise from the noisy codeword to get the denoised codeword. This scheme is hereafter referred to as DNNet-NEU.

The impact of a noisy CSI on the BER and secrecy capacity of a PLS scheme that combines matched filter (MF) precoding and diversity was investigated in [10]. The conclusion was that as the CSI error variance increases, the secrecy capacity reduces and BER significantly increases leading to system degradation. In this paper, a neural network denoising algorithm that is employed at the transmitter to denoise the imperfect CSI is introduced. The denoised CSI is then used for the MF precoding and ensures Bob retains the intended security gains over Eve. The contributions of this paper include:

- We propose a denoising deep autoencoder model referred to as DenoiseSecNet. This model accepts noisy CSI as input and gives denoised CSI that are nearly accurate estimates of the noiseless CSI.

This work was funded by Institut Supérieur d'Électronique de Paris (ISEP) and Agence Nationale des Fréquences (ANFR).

- We propose a hybrid model (HybDenoiseSecNet) that combines a conventional denoising scheme with a shallow denoising autoencoder. This achieved the same performance as DenoiseSecNet but at a much-reduced complexity.
- Numerical results show the BER and secrecy capacity performance improvement of the proposed schemes over legacy denoising schemes.
- We also show the significant reduction in complexity of our proposed scheme compared to another neural network scheme in the literature.
- We investigate the impact of the choice of the activation function (AF) on the efficacy of the proposed models. We also study the performance of the models for different magnitudes of CSI error variances.

The rest of this paper is organized as follows: Section II is devoted to describing the system model of the PLS scheme that incorporates DenoiseSecNet/HybDenoiseSecNet. In Section III, the proposed models are presented. Simulation results are discussed in Section IV while Section V concludes the paper.

Notations: Individual vector elements, vectors, and matrices are denoted by normal letters (e.g. x), lowercase boldface letters (e.g. $\boldsymbol{x}$), and uppercase boldface letters (e.g. $\boldsymbol{X}$). Absolute, conjugate and l_2-norm are symbolized by $|x|$, x^*, and $\|\boldsymbol{x}\|_2$ respectively.

II. System Model

A. System Model

We consider an OFDM transmission with N subcarriers operating in FDD mode. The entries of the main channel between Alice and bob, $\boldsymbol{h^{(b)}}$, and the wiretap channel between Alice and Eve, $\boldsymbol{h^{(e)}}$, are independent and identically distributed (i.i.d.) Rayleigh fading zero-mean complex Gaussian variables with unit variance. For all pairs of uncorrelated subcarriers in the same OFDM block, ($h_{n_1}^{(b)}$ and $h_{n_2}^{(b)}$), Alice transmits MF precoded symbols, x_{n_1} and x_{n_2}, to Bob. To ensure the uncorrelation between subcarrier pairs, all pairs are chosen as follows:

$$h|_{n_1,n_2} = \begin{cases} h_{n_1}, & \text{where } 1 \leq n_1 \leq N/2, \\ h_{n_2}, & \text{where } n_2 = n_1 + N/2. \end{cases} \quad (1)$$

This is explained in Section IV-A. The instantaneous CSI of the main channel is used to design the precoder which maximizes signal-to-noise ratio (SNR) in the direction of Bob only. Frequency diversity is also added to improve reliability. The end-to-end transmission steps are shown in Fig. 1.

Eve is aware of the main channel CSI due to CSI feedback in FDD mode. Bob and Eve are located at separate locations. Hence, their channels exhibit uncorrelated propagation in a rich scattering environment [11]. This ensures that the intercepted transmit MF precoded signal is not optimal for Eve. It loses the diversity gain because the precoding was done with a CSI that is uncorrelated to its own. This provides secrecy capacity and BER gain for Bob over Eve.

For each pair of subcarriers, the received signals at Bob are such that

$$y_{n_1}^{(b)} = \quad h_{n_1}^{(b)} x_{n_1} + z_{n_1}^{(b)}, \qquad y_{n_2}^{(b)} = \quad h_{n_2}^{(b)} x_{n_2} + z_{n_2}^{(b)}, \quad (2)$$

where $z_{n_1}^{(b)}$ and $z_{n_2}^{(b)}$ are the random noise which are i.i.d. random Gaussian complex variables $\mathcal{CN}(0, \sigma^2)$.

The received signals at Eve are expressed as

$$y_{n_1}^{(e)} = \quad h_{n_1}^{(e)} x_{n_1} + z_{n_1}^{(e)}, \qquad y_{n_2}^{(e)} = \quad h_{n_2}^{(e)} x_{n_2} + z_{n_2}^{(e)}. \quad (3)$$

Similarly, $z_{n_1}^{(e)}$ and $z_{n_2}^{(e)}$ are the random noise which are i.i.d. random Gaussian complex variables $\mathcal{CN}(0, \sigma^2)$.

The MF-precoded signals for the transmit symbol, s, are expressed as

$$x_{n_1} = P_{n_1} s, \quad x_{n_2} = P_{n_2} s \quad (4)$$

where

$$P_{n_1} = \frac{\sqrt{2} h_{n_1}^{(b)^*}}{\sqrt{|h_{n_1}^{(b)}|^2 + |h_{n_2}^{(b)}|^2}}, \quad P_{n_2} = \frac{\sqrt{2} h_{n_2}^{(b)^*}}{\sqrt{|h_{n_1}^{(b)}|^2 + |h_{n_2}^{(b)}|^2}}. \quad (5)$$

B. Impact of Imperfect CSI

To study the impact of imperfect CSI, we assume a noisy feedback channel between Alice and Bob. The effect of this is that Alice precodes the symbol using a noisy CSI and thus the SNR for the legitimate user is no longer maximized. We model the imperfect CSI as given in [12]:

$$\boldsymbol{h}^{(b)} = \sqrt{1-\epsilon}\tilde{\boldsymbol{h}}^{(b)} + \sqrt{\epsilon}\boldsymbol{\psi}, \quad (6)$$

where $\boldsymbol{h}^{(b)}$ is the actual channel gain without errors and $\tilde{\boldsymbol{h}}^{(b)}$ is the imperfect channel gain with errors. The CSI error $\boldsymbol{\psi}$ is a zero-mean unit variance complex Gaussian random variable $C\mathcal{N}(0,1)$, and the magnitude of the error variance, $\epsilon \in [0, 1[$.nThe case $\epsilon = 0$ corresponds to the perfect CSI scenario while $\epsilon = 1$ corresponds to completely noisy CSI. Inspired by [10], the expressions for the performance metrics of the system under imperfect CSI conditions are hereafter expressed. For Bob, the instantaneous SNR, conditional BER, and conditional channel capacity using the QPSK constellation can be expressed respectively as:

$$\gamma^{(b)} = \frac{(1-\epsilon)(|\tilde{h}_{n_1}^{(b)}|^2 + |\tilde{h}_{n_2}^{(b)}|^2)\bar{\gamma}}{\epsilon\bar{\gamma} + 1}, \quad (7)$$

$$\mathrm{BER}^{(\mathrm{b})}\Big|_{h_{n_1}^{(b)}, h_{n_2}^{(b)}} = \frac{1}{2}\mathrm{erfc}\left(\sqrt{\frac{\gamma^{(\mathrm{b})}}{2}}\right), \quad (8)$$

$$\mathrm{C}^{(\mathrm{b})}\Big|_{h_{n_1}^{(b)}, h_{n_2}^{(b)}} = \frac{1}{2}\log_2(1+\gamma^{(b)}), \quad (9)$$

where $\bar{\gamma}$ is the average SNR at the receiver. For asymptotic analysis, we consider the instantaneous SNR with imperfect CSI when $\bar{\gamma} \to \infty$. The asymptotic limit is given as

$$\lim_{\bar{\gamma}\to\infty} \gamma^{(b)} = \frac{(1-\epsilon)}{\epsilon}(|\tilde{h}_{n_1}^{(b)}|^2 + |\tilde{h}_{n_2}^{(b)}|^2). \quad (10)$$

The instantaneous SNR in this region is no longer dependent on the average SNR but is now limited by the CSI error variance. The implication of this is an error floor as will be

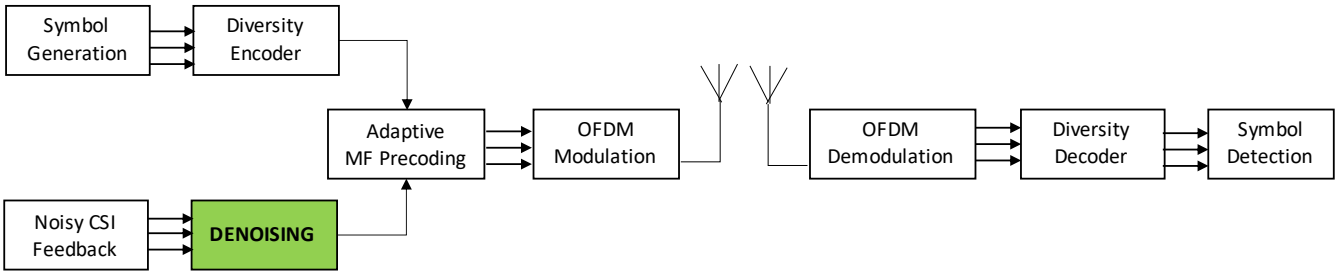

Fig. 1: System model for PLS Scheme that combines matched filter precoding and frequency diversity for security.

seen in section Section IV-A.

Similarly, for Eve, the instantaneous SNR, conditional BER, and conditional channel capacity using the QPSK constellation are given respectively:

$$\gamma^{(e)} = \frac{(1-\epsilon)(\beta\beta^*)\bar{\gamma}}{(\epsilon\bar{\gamma}+1)(|h_{n_1}^{(e)}|^2 + |h_{n_2}^{(e)}|^2)}, \tag{11}$$

$$\mathrm{BER}^{(e)}\Big|_{h_{n_1}^{(e)},h_{n_2}^{(e)}} = \frac{1}{2}\mathrm{erfc}\left(\sqrt{\frac{\gamma^{(e)}}{2}}\right), \tag{12}$$

$$\mathrm{C}^{(e)}\Big|_{h_{n_1}^{(e)},h_{n_2}^{(e)}} = \frac{1}{2}\log_2(1+\gamma^{(e)}), \tag{13}$$

where

$$\beta = h_{n_1}^{(e)}\tilde{h}_{n_1}^{(b)^*} + h_{n_2}^{(e)}\tilde{h}_{n_2}^{(b)^*}. \tag{14}$$

The secrecy capacity is the positive difference between the channel capacities of Bob (9) and Eve (13). The final BER and secrecy capacity are obtained by averaging the conditional ones on the variables h_{n_1} h_{n_2} for all subcarrier pairs in N.

III. Proposed Scheme

A. Structure and Operation of DenoiseSecNet

In this paper, to denoise the imperfect CSI at the transmitter, we have used the feed-forward autoencoder of deep learning, a very well-known model in deep learning [13]. DenoiseSecNet is a 5-layer autoencoder block consisting of the input layer, output layer, and 3 hidden layers as shown in Fig. 2. We define $f(.)$ and $g(.)$ as the encoder and decoder operations of the autoencoder respectively. In DenoiseSecNet, we define the input as the noisy CSI, $\tilde{\boldsymbol{h}}$. Thus the encoder and decoder outputs will be $f(\tilde{\boldsymbol{h}})$ and $g(f(\tilde{\boldsymbol{h}}))$ respectively. The encoding and decoding operations both take place at Alice. Afterward, the output of the decoding block is used to precode the transmit signal.

Starting from the first hidden layer to the output layer, we have fully connected (FC) layers and an activation layer that provides non-linearity to the model. For the ℓ-th layer of the model, the linear activation can be written as:

$$\boldsymbol{m}_\ell = \boldsymbol{W}_\ell \boldsymbol{a}_{\ell-1} + \boldsymbol{b}_\ell, \tag{15}$$

where $\boldsymbol{a}_{\ell-1}$ is the activation of the previous $(\ell-1)$-th layer, $\boldsymbol{W}_\ell$ represents the weight of the current ℓ-th layer and $\boldsymbol{b}_\ell$ are the biases for the layer. Note that the noisy CSI is the input for the first layer, i.e. $\boldsymbol{a}_0 = \tilde{\boldsymbol{h}}$.

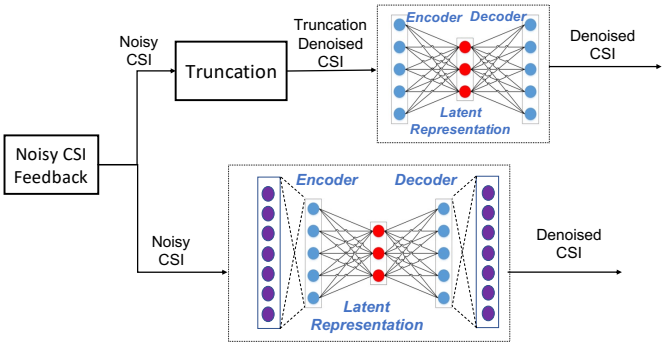

Fig. 2: Denoising ANN Autoencoder.

Next, we introduce non-linearity into the model. This is needed to develop complex representations that can properly model the function. Non-linearity is achieved by the use of AF and the AF of choice is the parametric rectified linear unit (PReLU). This AF improves model fitting with nearly zero extra computational cost and little overfitting risk [14]. The rationale behind choosing PReLU is explained in Section IV-A. PReLU is evaluated as:

$$\phi(m) = \begin{cases} m, & \text{if } m \geq 0, \\ \xi m, & otherwise. \end{cases}, \tag{16}$$

where ξ is a learnable parameter. The output of the encoder section of the model, labeled as "Latent Representation" in Fig. 2, is given below:

$$f(\tilde{\boldsymbol{h}}) = \phi_\ell(\boldsymbol{W}_\ell(\phi_{\ell-1}(...\phi_1(\boldsymbol{W}_1\tilde{\boldsymbol{h}} + \boldsymbol{b}_1))) + \boldsymbol{b}_\ell), \tag{17}$$

where $\phi(.)$ represents the non-linear activation. After encoding, the decoder takes the encoded data and generates an output that is an optimal match of the noiseless version of the noisy input. The decoder section is represented below:

$$g(f(\tilde{\boldsymbol{h}})) = \phi_L(\boldsymbol{W}_L(\phi_{\ell-1}(...\phi_1(\boldsymbol{W}_1 f(\tilde{\boldsymbol{h}}) + \boldsymbol{b}_1))) + \boldsymbol{b}_L). \tag{18}$$

To train the model, the hyperparameters were optimized using ray tune [15]. These include the number of layers and nodes per layer, the batch size, and the choice of the AF. The loss, $\mathcal{L}(h, g(f(\tilde{h})))$, is evaluated using MSE loss as:

$$\mathcal{L}(\boldsymbol{h}, g(f(\tilde{\boldsymbol{h}}))) = \frac{1}{N}\sum_{i=1}^{N}\|\hat{\boldsymbol{h}} - \boldsymbol{h}\|_2^2, \tag{19}$$

where $\hat{\boldsymbol{h}}$ is the output of the autoencoder. In this paper, MSE is preferred to mean absolute error (MAE) and mean

squared logarithmic error (MSLE) because we want to ensure that the large errors are significantly more penalized than the smaller errors. To optimize the system and iteratively update the parameters accordingly, we used the stochastic gradient descent (SGD) optimizer. It outperforms other optimizers such as Adam, RMSprop, Adagrad, AdaDelta, etc. in our work.

B. Hybrid Option of DenoiseSecNet

For complexity considerations, we propose a hybrid option to denoise the noisy CSI, HybDenoiseSecNet. The major motivation here is to obtain similar BER and secrecy capacity performance gains to DenoiseSecNet but at reduced complexity. To achieve this, the imperfect CSI is first denoised using the legacy scheme, truncation method, mentioned in Section I. We assume that the channel length is known at Alice due to feedback in FDD mode. Assuming N subcarriers and a known channel tap length of T, the noisy CSI feedback ($\tilde{\boldsymbol{h}}$) is first transformed from frequency domain to time domain (TD), as $\tilde{\boldsymbol{h}}^{TD}$, using inverse fast Fourier transform (IFFT) operation of size N. The truncation then takes place in the time domain as seen in (20).

$$\ddot{h}_t^{TD} = \begin{cases} \tilde{h}_t^{TD}, & \text{if } 0 \leq t \leq T-1, \\ 0, & \text{if } T \leq t \leq N. \end{cases}, \tag{20}$$

Channel taps beyond the known significant tap of T are assumed to be caused by the noise and are ignored. Then the truncated CSI is transformed to the frequency domain as, $\ddot{\boldsymbol{h}}$, using the fast Fourier transform (FFT). This denoised CSI is then passed through the ANN autoencoder for further denoising operation as seen in (21). Since already partially denoised, the ANN autoencoder can achieve a significant further reduction in noise with fewer computations as compared to the full option of DenoiseSecNet. In fact, we do not need a deep neural network and a shallow neural network can produce optimal results.

$$g(f(\ddot{\boldsymbol{h}})) = \phi_L(\boldsymbol{W}_L(\phi_{\ell-1}(...\phi_1(\boldsymbol{W}_1 f(\ddot{\boldsymbol{h}}) + \boldsymbol{b}_1))) + \boldsymbol{b}_L). \tag{21}$$

The proposed hybrid version is shown in Fig. 2. With other hyperparameters remaining similar, the change in the hybrid model is the number of hidden layers and neurons, and thus the model complexity.

IV. Result and Discussion

A. BER and Secrecy Capacity Performances

In this section, we present the performance of our proposed DenoiseSecNet and HybDenoiseSecNet and compare them to legacy denoising schemes. We consider an OFDM system with $N = 64$ subcarriers and a QAM constellation. The hidden layers for the full version of DenoiseSecNet are 64-16-64 while the hybrid version has only one 16-neuron hidden layer. The noisy CSI input of 64 subcarriers with 64 complex numbers each is separated into the real and imaginary components at the input and output of the model. Hence, the input and output layers are each 128 in length. The hyperparameters used in the simulation are summarized in Table I. For the DNNet-NEU scheme, we consider the hyperparameters as proposed by the authors in [8]. The Vehicular A model corresponding to a highly frequency selective radio environment with power delay profiles (PDPs) described in Table II is considered.

TABLE I: Hyperparameters

DenoiseSecNet Structure	128-64-16-64-128
HybDenoiseSecNet Structure	128-16-128
DNNet-NEU Structure	128-1024-128
Training Sample Size	7×10^5
Validation Sample Size	2×10^5
Test Sample Size	1×10^5
Batch size	20
Learning rate	0.01
Optimizer	SGD
CSI Error Variance	0.1
Loss Function	MSE

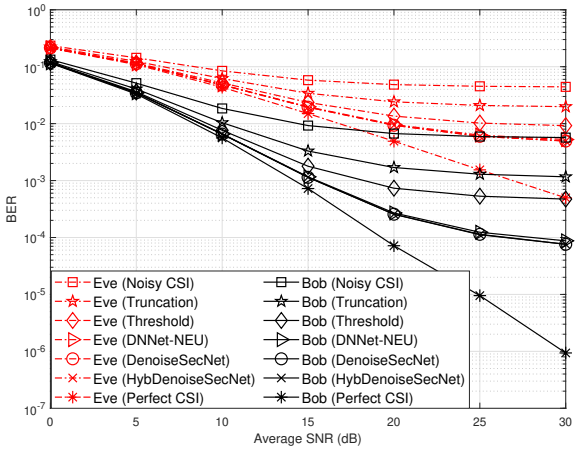

Fig. 3: BER performance of the proposed schemes compared to conventional schemes.

TABLE II: PDP for Vehicular-A with 10MHz Bandwidth: τ = delay spread and σ_t^2 = power

$\tau[ns]$	0	300	700	1100	1700	2500
$\sigma_t^2[dB]$	0	-1	-9	-10	-15	-20

From Table II, the coherence bandwidth, calculated as the inverse of multipath delay spread, is 2.7MHz [16]. From (1), this means there is a gap of 5MHz between subcarrier pairs and compared to a coherence bandwidth of 2.7MHz, uncorrelation between subcarriers is guaranteed.

In Fig. 3, the BER of Bob and Eve are plotted against the average SNR for different scenarios. When the CSI is perfect (ϵ = 0), Bob has a diversity gain of 2 but Eve loses the diversity gain. The higher BER at Eve leads to a security gap between Bob and Eve. With a noisy CSI ($\epsilon = 0.1$), the performances of Bob and Eve are completely degraded, and both exhibit error floors from an average SNR of 20 dB as explained in Section II-B. Evidently, the PLS scheme is highly sensitive to CSI accuracy. We then analyze the BER performance for the proposed autoencoder models (full and hybrid), DNNet-NEU, and two conventional non-neural network denoising schemes; universal threshold and

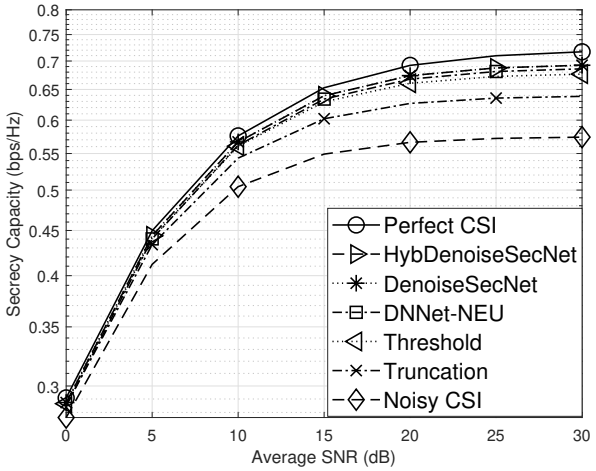

Fig. 4: Secrecy performance of the proposed schemes compared to conventional schemes.

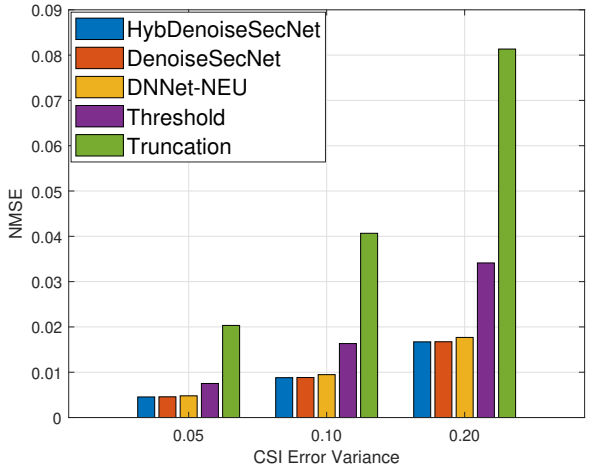

Fig. 5: NMSE performance at different error variance levels.

truncation schemes. We observe that the neural network-based schemes outperform the conventional schemes. Truncation and universal threshold schemes exhibit an error floor of 10^{-3} and 5×10^{-3} respectively around 30 dB average SNR. When DenoiseSecNet, HybDenoiseSecNet, and DNNet-NEU are used to denoise the noisy CSI, we can see a significant enhancement in BER performance. The two proposed models achieve the same level of BER less than 10^{-4} at SNR = 30dB. The BER performance of DNNet-NEU is approximately the same as that of the proposed models.

In Fig. 4, we see the secrecy capacity performance for the schemes. Expectedly, the secrecy capacity is highest under perfect CSI conditions and lowest when the CSI error variance is highest (ϵ = 0.1). The proposed schemes and DNNet-NEU have a secrecy capacity slightly below the best-case scenario. Again, the hybrid and full versions of DenoiseSecNet have the same performance. Next to this is the universal threshold scheme, and the truncation scheme was the least effective CSI denoising scheme. It should be noted that the secrecy capacity was positive in all the cases. This shows that despite the performance degradation due to the noisy CSI, the channel capacity of Bob remains higher than the channel capacity of Eve under similar conditions.

The performances of the denoising schemes are compared at three CSI error variance levels (ϵ = 0.05, 0.1, and 0.2) in Fig. 5. Again, DenoiseSecNet and its hybrid version had the lowest normalized mean squared error (NMSE) after denoising. The truncation scheme had the highest NMSE. The schemes remained equally effective in terms of the percentage reduction in error irrespective of the error variance. Compared to the initial CSI error variances, a 91% error reduction was achieved with full and hybrid versions of DenoiseSecNet, while DNNet-NEU, threshold, and truncation schemes achieved 90%, 85%, and 60% reductions respectively.

We compare the performance of HybDenoiseSecNet at ϵ=0.1 w.r.t. different AFs. We have chosen to use non-saturated AFs that have the advantage of solving the vanishing/exploding gradient problems while improving the convergence speed. Rectified linear unit (ReLU) had the highest NMSE, this can be explained by the fact that it only considers the positive part of the linear activation and ignores the negative. The CSI on the other hand has a distribution of positive and negative components. The second-highest NMSE of 0.49 was observed with leaky ReLU. By default, this AF assigns a gradient of 0.01 to the negative component of the linear activation but this does not optimally model our CSI distribution. Scaled exponential linear unit (SELU), a self-normalizing AF suitable for ANNs to enable high-level abstract representation [17] was also considered. Finally, the best performance was observed with PReLU. This is explained by the fact that the AF can learn the gradient for the negative region of the CSI. Hence, it properly captures the entire positive and negative ranges of the CSI.

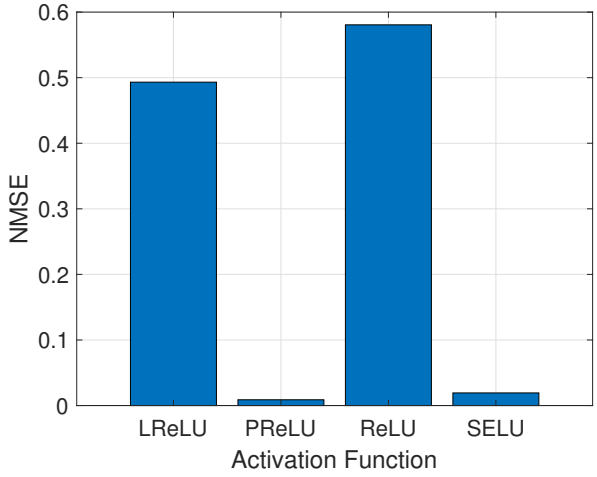

Fig. 6: NMSE performance of HybDenoiseSecNet w.r.t. AFs.

B. Computational Analysis

Inspired by [18], the computational complexity analysis is done in terms of the number of real-valued mathematical operations (multiplication/division and summation/subtraction) needed to denoise the noisy CSIs.

TABLE III: Computational Complexity in terms of real-valued operations

Denoising Scheme	# of Multiplications	# of Summations
Truncation	1,152	1,536
Universal Threshold	1,152	2,304
DenoiseSecNet	18,432	18,432
HybDenoiseSecNet	5,248	5,632
DNNet-NEU	262,144	262,144

For the truncation scheme, most of the complexity is from the IFFT operation before truncation and the FFT operation afterward. It is well known that the complexity of a single FFT operation is $(N/2)\log N$ complex multiplications and $N\log N$ complex summations. A complex multiplication is equivalent to 3 real-valued multiplications and 2 real-valued summations and a complex summation is equivalent to 2 real-valued summations. In essence, for the truncation scheme, the complexity is broken down to $3N\log N$ real-valued multiplications and $4N\log N$ real-valued summations. In the universal threshold denoising scheme, in addition to truncation, we have the two median calculations and signal clipping operations. This introduces an additional $2N\log N$ to make a total of $6N\log N$ real-valued operations [1]

For the neural network schemes, the focus is on the number of real-valued multiplications and summations required to activate all neurons in the hidden and output layers of the network. Moving from the ℓ-th to the $(\ell+1)$-th layer will require $J_\ell J_{\ell+1}$ multiplications/summations for the linear transformation, where J signifies the number of neurons in the layer. The extra operations are the bias summation and vector product in the activation. In summary, the real-valued multiplication and summation in DenoiseSecNet are given as:

$$\mathcal{N}_{MUL} = \mathcal{N}_{SUM} = \sum_{\ell=1}^{L} J_{\ell-1}J_\ell \tag{22}$$

Table III gives a summary of the number of real-valued operations for all the considered denoising schemes. From this table, we see that for both multiplication and summation operations, HybDenoiseSecNet requires only about 30% of the processing resources used by DenoiseSecNet. In other words, the full option uses 3.3 times more resources than the hybrid option. As expected, the hybrid option is more complex than the threshold and truncation schemes but the significant secrecy and BER performance gains are valid motivations to employ this scheme. However, DNNet-NEU requires the most amount of computational complexity and is 14 times the complexity of DenoiseSecNet and 50 times that of HybDenoiseSecNet. This significant reduction in complexity is what makes HybDenoiseSecNet an interesting alternative.

V. Conclusion

In this paper, we proposed two denoising autoencoder models (DenoiseSecNet and HybDenoiseSecNet) that are used to denoise noisy CSI in a channel adaptation PLS scheme. Through simulations, we showed that our scheme significantly outperforms conventional schemes in terms of BER, secrecy capacity, and NMSE. We also studied the reduced complexity of our proposed schemes compared to another neural network scheme in the literature. An interesting extension of this work will be to consider the multi-antenna scenario and cases where the noise variance is not uniform across subcarriers.

[1] Recall that median calculation involves sorting and the best sorting algorithms are at $N\log(N)$ complexity.

References

[1] J. M. Hamamreh, H. M. Furqan, and H. Arslan, "Classifications and applications of physical layer security techniques for confidentiality: A comprehensive survey," *IEEE Communications Surveys Tutorials*, vol. 21, no. 2, pp. 1773–1828, 2019.

[2] P. Sure and C. M. Bhuma, "A survey on OFDM channel estimation techniques based on denoising strategies," *Engineering Science and Technology, an International Journal*, vol. 20, no. 2, pp. 629–636, 2017.

[3] Z. Xiao, Z. Mingtong, and W. Chengyou, "Iterative threshold channel estimation in ORGV convolutional code MISO-OFDM system," *IETE Technical Review*, p. 1–16, 2021.

[4] H. Xie, G. Andrieux, Y. Wang, J.-F. Diouris, and S. Feng, "Efficient time domain threshold for sparse channel estimation in OFDM system," *International Journal of Electronics and Communications*, vol. 68, no. 4, Apr. 2014.

[5] S. Tuffery, "Deep learning: From big data to artificial intelligence with R: Deep learning for natural language processing," pp. 431–478, 2023.

[6] N. Le, V. S. Rathour, K. Yamazaki, K. Luu, and M. Savvides, "Deep reinforcement learning in computer vision: a comprehensive survey," *Artificial Intelligence Review*, vol. 55, no. 4, pp. 2733–2819, 2022.

[7] T. Zhou, H. Zhang, B. Ai, C. Xue, and L. Liu, "Deep-learning-based spatial–temporal channel prediction for smart high-speed railway communication networks," *IEEE Transactions on Wireless Communications*, vol. 21, no. 7, pp. 5333–5345, 2022.

[8] H. Ye, F. Gao, J. Qian, H. Wang, and G. Y. Li, "Deep learning-based denoise network for csi feedback in FDD massive MIMO systems," *IEEE Communications Letters*, vol. 24, no. 8, pp. 1742–1746, 2020.

[9] V. Rizzello and W. Utschick, "Learning the CSI denoising and feedback without supervision," in *2021 IEEE 22nd International Workshop on Signal Processing Advances in Wireless Communications (SPAWC)*, 2021, pp. 16–20.

[10] I. Ajayi, Y. Medjahdi, F. Kaddour, and L. Mroueh, "Impact of imperfect channel state information on physical layer security by precoding and diversity," in *2021 8th International Conference on Electrical Engineering, Computer Science and Informatics (EECSI)*, 2021, pp. 322–327.

[11] F. Pan, Z. Pang, M. Luvisotto, M. Xiao, and H. Wen, "Physical-layer security for industrial wireless control systems: Basics and future directions," *IEEE Industrial Electronics Magazine*, vol. 12, no. 4, pp. 18–27, 2018.

[12] M. A. A. Hyadi, Z. Rezki, "An overview of physical layer security in wireless communication systems with CSIT uncertainty," *The Bell System Technical Journal*, vol. 4, pp. 6121– 6132, 2016.

[13] Y. Bengio, L. Yao, G. Alain, and P. Vincent, "Generalized denoising auto-encoders as generative models," in *26th International Conference on Neural Information Processing Systems*, ser. NIPS'13, vol. 1, 2013, p. 899–907.

[14] K. He, X. Zhang, S. Ren, and J. Sun, "Delving deep into rectifiers: Surpassing human-level performance on imagenet classification," in *2015 IEEE International Conference on Computer Vision (ICCV)*, 2015, pp. 1026–1034.

[15] R. Liaw, E. Liang, R. Nishihara, P. Moritz, J. E. Gonzalez, and I. Stoica, "Tune: A research platform for distributed model selection and training," *arXiv preprint arXiv:1807.05118*, 2018.

[16] A. Goldsmith and K. (Firm), *Wireless Communications*, ser. Cambridge Core. Cambridge University Press, 2005. [Online]. Available: https://books.google.fr/books?id=n-3ZZ9i0s-cC

[17] G. Klambauer, T. Unterthiner, A. Mayr, and S. Hochreiter, "Self-normalizing neural networks," in *26th International Conference on Neural Information Processing Systems*, vol. 1, 2017, p. 899–907.

[18] A. K. Gizzini, M. Chafii, A. Nimr, and G. Fettweis, "Deep learning based channel estimation schemes for IEEE 802.11p standard," *IEEE Access*, vol. 8, pp. 113 751–113 765, 2020.